Tunneling of coupled methyl groups in lithium acetate: The isotope effect

A. Heidemann [1], H. Friedrich [2], E. Günther [2], and W. Häusler [3]

[1] Institut Laue-Langevin, Grenoble, France
[2] Physikalisch-Technische Bundesanstalt, Braunschweig, Federal Republic of Germany
[3] Institut für Theoretische Physik I, Universität Erlangen-Nürnberg, Erlangen, Federal Republic of Germany

We studied by high resolution inelastic neutron scattering the isotope effect of tunneling of coupled methyl groups in lithium acetate dihydrate (LIAC). Fully protonated, fully deuterated and mixed LIAC samples were investigated. The results are described by a simple model in which it is assumed that the single particle potential hindering rotation is strongly increased by deuteration, whereas the coupling potential is nearly unchanged. This allows to interpret the very strong isotope effect and also the spectra of the mixed compounds. The strong increase of the single particle potential by deuteration is tentatively explained by phonon mediated coupling.

1. Introduction

Rotational tunneling of methyl groups in Lithium acetate (LIAC) has been studied in the past in detail experimentally and theoretically [1 to 7]. The reason for the interest in this compound is the fact that it is *the* model system for coupled pairs of methyl groups. The crystal structure of fully protonated LIAC (CH_3 COOLi. $2H_2O$) was determined by single crystal X-ray diffraction at room temperature by Galigné et al. [8]. The structure is orthorhombic with space group *Cmmm*. No phase transition is reported to occur down to liquid helium temperatures. The CH_3 groups occur in pairs (distance 2.5 Å) with a common axis of rotation along the *b* axis. The distance between nearest pair axes is 6.6 Å. The tunneling spectrum and its temperature and pressure dependence have been studied by inelastic neutron scattering (INS) [3–5]. The methyl-methyl coupling manifests itself by the lineshape of the spectra which is more complicated than in a system with uncoupled groups.

A theoretical explanation of the INS results has first been given by Clough et al. [3] and later by Häusler and Hüller [7]. In both cases the coupled pair is described by a simple model Hamiltonian:

$$H = H_1 + H_2 + H_{12} \tag{1}$$

with

$$H_i = -B_i \frac{\partial^2}{\partial \phi_i^2} + V_3 \cos 3\phi_i$$

and

$$H_{12} = W_3 \cos 3(\phi_1 - \phi_2) \tag{2}$$

ϕ_i and B_i are the rotational coordinates and rotational constants:

$$B = \frac{\hbar^2}{2I} = \begin{cases} 647.5\,\mu\text{eV} & \text{for } CH_3 \text{ groups} \\ 323.7\,\mu\text{eV} & \text{for } CD_3 \text{ groups} \end{cases}$$

I is the moment of inertia. We neglect bond length differences between CH_3 and CD_3 groups.

Expression (2) for the interaction potential of a pair of coupled methyl groups is the simplest, one can write down. The Schrödinger equation with Hamiltonian H can be solved numerically to any desired

degree of accuracy [3, 7]. A parameter pair (V_3, W_3) which describes well the tunneling spectra of CH_3 groups in LIAC was obtained [3]:

$$V_3 = 2.96\, B_{\text{proton}},$$

$$W_3 = -6.58\, B_{\text{proton}}.$$

By simple scaling with the rotational constants we can predict on the basis of these values the tunneling frequencies of deuterated pairs to be around 25 μeV compared to values near 270 μeV for protonated pairs. This isotope effect is even stronger than it would be for single methyl groups due to the non frustrated type of coupling ($W_3 < 0$): An orientationally more strongly localised deuterated neighbour deepens the averaged potential at a certain methyl site.

The isotope effect on methyl tunneling has already been studied in a number of other compounds which however do not exhibit coupling effects [9–12]. Methane is a system where coupling effects were observed [13] and where the isotope effect has also been studied [14]. The latter is however strongly influenced by the fact that the crystal structures of CH_4 and CD_4 are quite different at low temperatures leading in this case to spectra for the two species with completely different shapes.

The aim of the experiments presented in this paper was to study the isotope effect in LIAC by INS to gain more detailed information about the potential barriers hindering rotation. We investigated both isotopically pure and mixed samples of polycrystalline LIAC.

In Sect. 2 we present some theoretical aspects about tunnel splittings and spectra of protonated, deuterated and mixed methyl pairs. The experiments and results are described and discussed in Sects. 3 and 4.

2. Theory

2.1. *Spin states of single* CD_3 *groups*

The CD_3 groups has $(2I+1)^3 = 27$ different spin states ($I_{\text{deuteron}} = 1$). They have either A, E^a or E^b symmetry [15]. From the three one-deuteron spin states $|\uparrow\rangle$, $|0\rangle$, $|\downarrow\rangle$ we can construct the 27 spin states $|\Gamma; I, I^z\rangle$ of CD_3 which have to be eigenstates of the z-component I_z and the square I^2 of the total angular momentum operator. Γ is either A, E^a or E^b. The 27 spin states of CD_3 are given in Table 1 ($\varepsilon = \exp(i\, 2\pi/3)$).

2.2. *Transition probabilities for the inelastic and quasielastic peaks of neutron scattering from single* CD_3 *groups*

The spin incoherent part of the neutron scattering operator W can be written down in a symmetry-adapted form [16, 17]:

$$W = \tfrac{1}{3} \sum_{\Gamma} W^{\Gamma}, \qquad W^{\Gamma} = W^{\Gamma}_{\text{spatial}} \cdot W^{\Gamma *}_{\text{spin}} \tag{3}$$

(* stands for Hermitian conjugate)

$$W^{\Gamma}_{\text{spatial}} = a_s \sum_{j=1}^{3} \chi^j \, e^{i\mathbf{Q}\cdot\mathbf{R}_j}, \tag{4}$$

$$W^{\Gamma}_{\text{spin}} = \frac{2}{\sqrt{I(I+1)}} \sum_{j=1}^{3} \chi^j \mathbf{S}\cdot\mathbf{I}_j, \tag{5}$$

$$\chi = \begin{Bmatrix} 1 & \text{for } \Gamma = A \\ \varepsilon & \text{for } \Gamma = E^a \\ \varepsilon^* & \text{for } \Gamma = E^b \end{Bmatrix}. \tag{6}$$

$\mathbf{S}$ is the neutron spin operator, a_s the spin dependent scattering length, $\mathbf{Q}$ the momentum transfer and $\mathbf{R}_j$ the position operator.

W^A is responsible for transitions in which the methyl group does not change its spin symmetry and it therefore gives rise to the elastic peak. W^{Ea} and W^{Eb} are responsible for the inelastic and quasielastic peaks [16].

The double differential cross section for neutron scattering is given by:

$$\frac{d^2\sigma}{d\Omega\, d\omega} = \frac{k'}{k} \sum_{\substack{n,\Gamma,I,I^z,\mu \\ n',\Gamma',I',I^{z'},\mu'}} P_\mu P_{n\Gamma II^z} \cdot |\langle \mu' | \langle \Gamma'; I', I^{z'} | \langle n'; \Gamma' | W^{\Gamma''} | n; \Gamma \rangle | \Gamma; I, I^z \rangle | \mu \rangle|^2 \cdot \delta(\hbar\omega + E^{\Gamma}_n - E^{\Gamma'}_{n'}) \tag{7}$$

where k, k' are the moduli of the initial and final neutron wave vectors, $|\mu\rangle$ is the neutron spin state, P_μ its initial statistical weight. $|n; \Gamma\rangle$ denotes the spatial state of the molecule, $P_{n\Gamma II^z}$ the statistical weight for the initial state. E^{Γ}_n and $E^{\Gamma'}_{n'}$ denote initial and final energy eigenvalues respectively. For unpolarized neutrons $P_\mu = 1/2$ and for an unpolarized sample, i.e. $P_{n\Gamma II^z}$ not depending on I and I^z, we have:

$$\frac{d^2\sigma}{d\Omega\, d\omega} = \frac{k'}{k} \sum_{\substack{n,\Gamma \\ n',\Gamma'}} P_{n\Gamma} |\langle n'; \Gamma' | W^{\Gamma''}_{\text{spatial}} | n; \Gamma \rangle|^2 \cdot S_{\Gamma'\Gamma}\, \delta(\hbar\omega + E^{\Gamma}_n - E^{\Gamma'}_{n'}) \tag{8}$$

Table 1. Simultaneous eigenstates of $\hat{I}^z := \hat{I}_1^z + \hat{I}_2^z + \hat{I}_3^z$ and of $\hat{I}^2 := (\hat{I}_1 + \hat{I}_2 + \hat{I}_3)^2$, correctly symmetrized with respect to the even permutations of the 3 spins

$\|i\rangle$	$\|\Gamma\ I\ I_z\rangle$	CD_3-spin-function
1	$A\ 3\ 3$	$\|\uparrow\uparrow\uparrow\rangle$
2	$A\ 3\ 2$	$(\|\uparrow\uparrow 0\rangle + \|\uparrow 0\uparrow\rangle + \|0\uparrow\uparrow\rangle)/\sqrt{3}$
3	$A\ 3\ 1$	$[\|\uparrow\uparrow\downarrow\rangle + \|\uparrow\downarrow\uparrow\rangle + \|\downarrow\uparrow\uparrow\rangle + 2(\|00\uparrow\rangle + \|0\uparrow 0\rangle + \|\uparrow 00\rangle)]/\sqrt{15}$
4	$A\ 3\ 0$	$(\|0\uparrow\downarrow\rangle + \|\uparrow\downarrow 0\rangle + \|\downarrow 0\uparrow\rangle + \|0\downarrow\uparrow\rangle + \|\downarrow\uparrow 0\rangle + \|\uparrow 0\downarrow\rangle + 2\|000\rangle)/\sqrt{10}$
5	$A\ 3\ -1$	analog to functions with $I_z = +1, 2, 3$
6	$A\ 3\ -2$	
7	$A\ 3\ -3$	
8	$A\ 1\ 1$	$[2(\|\uparrow\uparrow\downarrow\rangle + \|\uparrow\downarrow\uparrow\rangle + \|\downarrow\uparrow\uparrow\rangle) - \|00\uparrow\rangle - \|0\uparrow 0\rangle - \|\uparrow 00\rangle]/\sqrt{15}$
9	$A\ 1\ 0$	$(\|\uparrow\downarrow 0\rangle + \|\downarrow 0\uparrow\rangle + \|0\uparrow\downarrow\rangle + \|\downarrow\uparrow 0\rangle + \|\uparrow 0\downarrow\rangle + \|0\downarrow\uparrow\rangle - 3\|000\rangle)/\sqrt{15}$
10	$A\ 1\ -1$	analog to function with $I_z = 1$
11	$A\ 0\ 0$	$(\|\uparrow\downarrow 0\rangle - \|\downarrow\uparrow 0\rangle + \|\downarrow 0\uparrow\rangle - \|\uparrow 0\downarrow\rangle + \|0\uparrow\downarrow\rangle - \|0\downarrow\uparrow\rangle)/\sqrt{6}$
12	$E^a\ 2\ 2$	$(\|\uparrow\uparrow 0\rangle + \varepsilon\|\uparrow 0\uparrow\rangle + \varepsilon^*\|0\uparrow\uparrow\rangle)/\sqrt{3}$
13	$E^a\ 2\ 1$	$(\|\uparrow\uparrow\downarrow\rangle + \varepsilon\|\uparrow\downarrow\uparrow\rangle + \varepsilon^*\|\downarrow\uparrow\uparrow\rangle - \|00\uparrow\rangle - \varepsilon\|0\uparrow 0\rangle - \varepsilon^*\|\uparrow 00\rangle)/\sqrt{6}$
14	$E^a\ 2\ 0$	$(\|0\uparrow\downarrow\rangle - \|0\downarrow\uparrow\rangle + \varepsilon\|\uparrow\downarrow 0\rangle - \varepsilon\|\downarrow\uparrow 0\rangle + \varepsilon^*\|\downarrow 0\uparrow\rangle - \varepsilon^*\|\uparrow 0\downarrow\rangle) \cdot \frac{1-\varepsilon^*}{3\sqrt{2}}$
15	$E^a\ 2\ -1$	analog to functions with $I_z = 1, 2$
16	$E^a\ 2\ -2$	
17	$E^a\ 1\ 1$	$(\|\uparrow\uparrow\downarrow\rangle + \varepsilon\|\uparrow\downarrow\uparrow\rangle + \varepsilon^*\|\downarrow\uparrow\uparrow\rangle + \|00\uparrow\rangle + \varepsilon\|0\uparrow 0\rangle + \varepsilon^*\|\uparrow 00\rangle)/\sqrt{6}$
18	$E^a\ 1\ 0$	$(\|0\uparrow\downarrow\rangle + \|0\downarrow\uparrow\rangle + \varepsilon\|\uparrow\downarrow 0\rangle + \varepsilon\|\downarrow\uparrow 0\rangle + \varepsilon^*\|\downarrow 0\uparrow\rangle + \varepsilon^*\|\uparrow 0\downarrow\rangle) \cdot \frac{1+\varepsilon^*}{\sqrt{6}}$
19	$E^a\ 1\ -1$	analog to function with $I_z = 1$
20	$E^b\ 2\ 2$	analog to functions $\|E^a\ I\ I_z\rangle$ with ε replaced by ε^* and vice versa, $\varepsilon = \exp(i\,2\pi/3)$
21	$E^b\ 2\ 1$	
22	$E^b\ 2\ 0$	
23	$E^b\ 2\ -1$	
24	$E^b\ 2\ -2$	
25	$E^b\ 1\ 1$	
26	$E^b\ 1\ 0$	
27	$E^b\ 1\ -1$	

Table 2. Elements of the matrix $M_{\alpha\alpha'} := \sum_{\mu,\mu'} P_\mu |\langle\mu|\langle\alpha| W_{\text{spin}} |\alpha'\rangle|\mu'\rangle|^2$ where $|\mu\rangle$ denote the spin states of the neutrons, $P_\mu = 1/2$ for unpolarized neutrons, $\alpha = 1, \ldots, 27$ enumerates the spin states of the CD_3 group

$\|\Gamma$	I	$I_z\rangle$	$\|\alpha\rangle$	1	2	3	4	5	6	7	8	9	10	11	12	13	14	15	16	17	18	19	20	21	22	23	24	25	26	27
A	3	3	1	9/2	3/2	0	0	0	0	0	0	0	0	0	3/2	0	0	0	0	0	0	0	3/2	0	0	0	0	0	0	0
A	3	2	2	3/2	2	5/2	0	0	0	0	0	0	0	0	1/2	1	0	0	0	0	0	0	1/2	1	0	0	0	0	0	0
A	3	1	3	0	5/2	1/2	3	0	0	0	0	0	0	0	1/10	4/5	3/5	0	0	0	0	0	1/10	4/5	3/5	0	0	0	0	0
A	3	0	4	0	0	3	0	3	0	0	0	0	0	0	0	3/10	9/10	3/10	0	0	0	0	0	3/10	9/10	3/10	0	0	0	0
A	3	−1	5	0	0	0	3	1/2	5/2	0	0	0	0	0	0	0	0	0	0	0	0	0	0	0	3/5	4/5	1/10	0	0	0
A	3	−2	6	0	0	0	0	5/2	2	3/2	0	0	0	0	0	0	0	0	0	0	0	0	0	0	0	1	1/2	0	0	0
A	3	−3	7	0	0	0	0	0	3/2	9/2	0	0	0	0	0	0	0	0	0	0	0	0	0	0	0	0	3/2	0	0	0
A	1	1	8	0	0	0	0	0	0	0	1/2	1/2	0	0	9/10	9/20	3/20	0	0	5/4	5/4	0	9/10	9/20	3/20	0	0	5/4	5/4	0
A	1	0	9	0	0	0	0	0	0	0	1/2	0	1/2	0	0	9/20	3/5	9/20	0	5/4	0	5/4	0	9/20	3/5	9/20	0	5/4	0	5/4
A	1	−1	10	0	0	0	0	0	0	0	0	1/2	1/2	0	0	0	3/20	9/20	9/10	0	5/4	5/4	0	0	3/20	9/20	9/10	0	5/4	5/4
A	0	0	11	0	0	0	0	0	0	0	0	0	0	0	0	0	0	0	0	3/2	3/2	3/2	0	0	0	0	0	3/2	3/2	3/2
E^a	2	2	12	3/2	1/2	1/10	0	0	0	0	9/10	0	0	0	2	1	0	0	0	0	0	0	1/2	1/4	0	0	0	9/4	0	0
E^a	2	1	13	0	1	4/5	3/10	0	0	0	9/20	9/20	0	0	1	1/2	3/2	0	0	0	0	0	1/4	1/8	3/8	0	0	9/8	9/8	0
E^a	2	0	14	0	0	3/5	9/10	3/5	0	0	3/20	3/5	3/20	0	0	3/2	0	3/2	0	0	0	0	0	3/8	0	3/8	0	3/8	3/2	3/8
E^a	2	−1	15	0	0	0	3/10	4/5	1	0	0	9/20	9/20	0	0	0	3/2	1/2	1	0	0	0	0	0	3/8	1/8	1/4	0	9/8	9/8
E^a	2	−2	16	0	0	0	0	1/10	1/2	3/2	0	0	9/10	0	0	0	0	1	2	0	0	0	0	0	0	1/4	1/2	0	0	9/4
E^a	1	1	17	0	0	0	0	0	0	0	5/4	5/4	0	3/2	0	0	0	0	0	1/2	1/2	0	9/4	9/8	3/8	0	0	1/8	1/8	0
E^a	1	0	18	0	0	0	0	0	0	0	5/4	0	5/4	3/2	0	0	0	0	0	1/2	0	1/2	0	9/8	3/2	9/8	0	1/8	0	1/8
E^a	1	−1	19	0	0	0	0	0	0	0	0	5/4	5/4	3/2	0	0	0	0	0	0	1/2	1/2	0	0	3/8	9/8	9/4	0	1/8	1/8
E^b	2	2	20	3/2	1/2	1/10	0	0	0	0	9/10	0	0	0	1/2	1/4	0	0	0	9/4	0	0	2	1	0	0	0	0	0	0
E^b	2	1	21	0	1	4/5	3/10	0	0	0	9/20	9/20	0	0	1/4	1/8	3/8	0	0	9/8	9/8	0	1	1/2	3/2	0	0	0	0	0
E^b	2	0	22	0	0	3/5	9/10	3/5	0	0	3/20	3/5	3/20	0	0	3/8	0	3/8	0	3/8	3/2	3/8	0	3/2	0	3/2	0	0	0	0
E^b	2	−1	23	0	0	0	3/10	4/5	1	0	0	9/20	9/20	0	0	0	3/8	1/8	1/4	0	9/8	9/8	0	0	3/2	1/2	1	0	0	0
E^b	2	−2	24	0	0	0	0	1/10	1/2	3/2	0	0	9/10	0	0	0	0	1/4	1/2	0	0	9/4	0	0	0	1	2	0	0	0
E^b	1	1	25	0	0	0	0	0	0	0	5/4	5/4	0	3/2	9/4	9/8	3/8	0	0	1/8	1/8	0	0	0	0	0	0	1/2	1/2	0
E^b	1	0	26	0	0	0	0	0	0	0	5/4	0	5/4	3/2	0	9/8	3/2	9/8	0	1/8	0	1/8	0	0	0	0	0	1/2	0	1/2
E^b	1	−1	27	0	0	0	0	0	0	0	0	5/4	5/4	3/2	0	0	3/8	9/8	9/4	0	1/8	1/8	0	0	0	0	0		1/2	1/2

where

$$S_{\Gamma''\Gamma}=\tfrac{1}{9}\sum_{\substack{I,I^z,\mu\\ I',I^{z'},\mu'}}\tfrac{1}{2}$$
$$\cdot|\langle\mu'|\langle\Gamma';I',I^{z'}|W^{\Gamma''}_{\text{spin}}|\Gamma;I,I^z\rangle|\mu\rangle|^2. \tag{9}$$

The squared matrix elements of $W_{\text{spin}}=\sum_{\Gamma} W^{\Gamma}_{\text{spin}}$ are shown after summation over the neutron spin states in Table 2, the corresponding table for CH_3 groups can be found in [16]. Because the energy transfer for a certain transition does not depend on I or I^z but only on the symmetry of the initial and final state, we can sum over the quantum numbers I and I^z and end up with a 3×3 "spin matrix" $S_{\Gamma\Gamma'}$ determining the spin part of the transition intensities:

$$S_{\Gamma\Gamma'}(CD_3)=\begin{matrix}A & E^a & E^b\end{matrix}\begin{Bmatrix}5 & 3 & 3\\ 3 & 2 & 3\\ 3 & 3 & 2\end{Bmatrix}\begin{matrix}A\\ E^a\\ E^b.\end{matrix} \tag{10}$$

For comparison

$$S_{\Gamma\Gamma'}(CH_3)=\tfrac{1}{12}\begin{matrix}A & E^a & E^b\end{matrix}\begin{Bmatrix}10 & 4 & 4\\ 4 & 1 & 4\\ 4 & 4 & 1\end{Bmatrix}\begin{matrix}A\\ E^a\\ E^b\end{matrix} \tag{11}$$

Note that $\sum_{\Gamma,\Gamma'} S_{\Gamma\Gamma'}=\begin{Bmatrix}3 & \text{for } CH_3\\ 27 & \text{for } CD_3\end{Bmatrix}$.

This ensures that

$$\iint\frac{d^2\sigma}{d\Omega\,d\omega}d\Omega\,d\omega\equiv\sigma=3\cdot4\pi a_s^2. \tag{12}$$

The off-diagonal elements of $S_{\Gamma\Gamma'}$ are all equal (valid for CD_3 *and* CH_3 groups). For high orientational barriers $V_3>15\,B_{\text{proton}}$ the spatial matrix elements squared are practically independent of Γ [24]. Therefore in this case the neutron inelastic (AE transition) and quasielastic (E^aE^b transition) intensities for scattering between levels in the groundstate are nearly identical. This is valid for CD_3 *and* CH_3 groups (see Fig. 1).

2.3. *Transition probabilities for inelastic and quasielastic neutron scattering from pairs of coupled methyl groups*

We have to consider three different types of pairs:

a) Fully protonated pairs: CH_3-CH_3.

b) Fully deuterated pairs: CD_3-CD_3.

c) Mixed pairs: CH_3-CD_3.

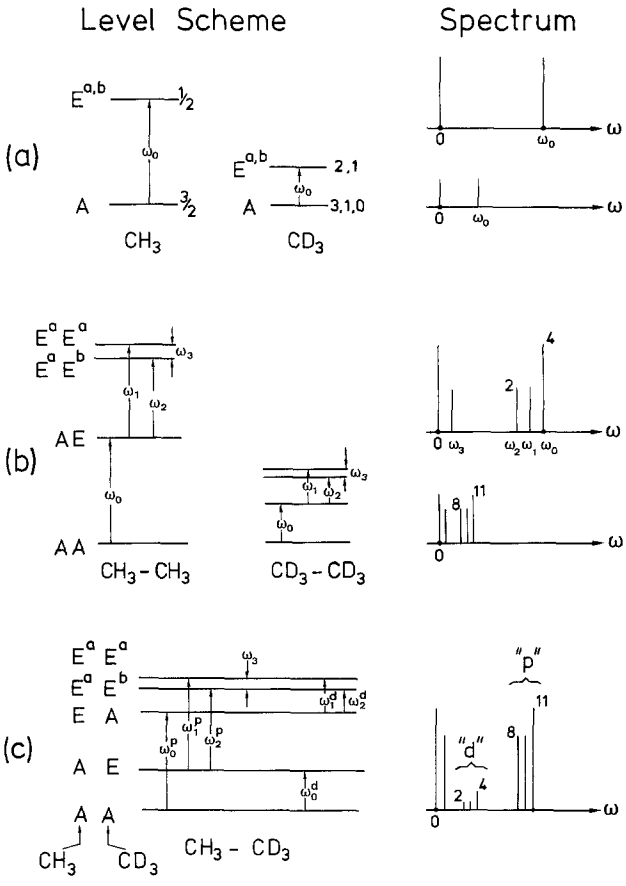

Fig. 1a–c. Level schemes and energy spectra of single CH_3 or CD_3 groups (**a**) and of equal (**b**) and mixed pairs (**c**) of methyl groups. The intensities reflect only spin space matrix elements. The "elastic" intensity shown in the spectra does not include transitions with no spin symmetry change

We can use the Hamiltonian (1) to calculate the eigenfrequencies of these pairs. Examples are given in Figs. 2 and 3 were the transition frequencies which can be excited by INS are plotted as a function of V_3 for a fixed parameter $W_3=-6.58\,B_{\text{proton}}$. As expected the highest frequencies belong to the CH_3-CH_3 pairs, the lowest to the CD_3-CD_3 pairs. Due to the non frustated coupling the mixed pair frequencies lie in between. Using the Hamiltonian (1) we assume that the coupling involves only spatial coordinates, the spin states of both groups remaining uncorrelated. This ensures that the spin dependent neutron scattering takes place at one of the two groups, the other averages out in its spin state. Therefore the intensity ratio between the different tunneling transitions is determined by the probability that the *neighbouring* methyl group is in the spin state Γ.

This probability is obtained by counting the number of A, E^a and E^b spin functions (for CD_3 groups see Table 1), and by assuming infinitely high spin temperatures:

$$A:E^a:E^b=\begin{cases}11:8:8 & \text{for } CD_3\\ 4:2:2 & \text{for } CH_3.\end{cases} \quad (13)$$

Assuming again no differences in spatial space for all symmetry changing groundstate transitions, we get the following intensity ratios for the neutron energy loss side (for notation of indices see Fig. 1):

$$I_0:I_1:I_2:I_3:I_{qu}=$$
$$\left\{\begin{array}{ll} 11:8\varepsilon_0^d:8\varepsilon_0^d:8\varepsilon_0^p\varepsilon_2^d:11\varepsilon_0^p & \text{for a } CH_3 \text{ group with a } CD_3 \text{ neighbour}\\ 11:8\varepsilon_0:8\varepsilon_0:8\varepsilon_0\varepsilon_2:11\varepsilon_0 & \text{for a } CD_3 \text{ group with a } CD_3 \text{ neighbour}\\ 4:2\varepsilon_0:2\varepsilon_0:2\varepsilon_0\varepsilon_2:\ 4\varepsilon_0 & \text{for a } CH_3 \text{ group with a } CH_3 \text{ neighbour}\\ 4:2\varepsilon_0^p:2\varepsilon_0^p:2\varepsilon_0^p\varepsilon_2^d:\ 4\varepsilon_0^d & \text{for a } CD_3 \text{ group with a } CH_3 \text{ neighbour}\end{array}\right\} \quad (14)$$

Here I_{qu} stands for the "quasielastic" intensity and ε_i is a Boltzmann factor:

$$\varepsilon_i=\exp(-\hbar\omega_i/k_BT).$$

We would like to mention that the intensity ratios (14) are now correct and erroneous results have been published earlier [3, 18, 19].

For the case of a mixed pair we get two scattering contributions, one from the deuterated, one from the protonated group of the pair. Assuming again high barriers, neglecting Boltzmann factors and normalizing the intensities such that scattering at the CD_3 groups yields $I_0:I_1:I_2:I_3:I_{qu}=4:2:2:2:4$, then the intensities for scattering at the CH_3 group are $\frac{11}{8}h:h:h:h:\frac{11}{8}h$, were $h=\frac{32}{27}(a_s^H/a_s^D)^2\simeq 57$. From this we see that the scattering at the CD_3 groups would hardly be detectable.

3. Experiments and results

Polycrystalline isotopic mixtures $Li^7(CH_3)_c(CD_3)_{1-c}\cdot 2D_2O$ with $c=0.0$, 0.05, 0.1, 0.2, 0.66, 0.8, 0.9 and 1.0 were prepared by solving weighted amounts of pure LIAC compounds in D_2O and by slow drying of the solutions in N_2 atmosphere at $\leqq 10$ °C. The samples were mounted in aluminium containers with the shape of hollow cylinders (height and outer diameter 30 mm, inner diameter variing between 0 and 29 mm depending on the degree of deuteration of the sample) in a temperature variable helium cryostat. The samples were cooled down from room temperature to 4 K within about one hour and kept at this temperature during the measurement period. The temperature stability was better than 0.02 K.

The inelastic neutron scattering experiments were carried out with the backscattering spectrometers

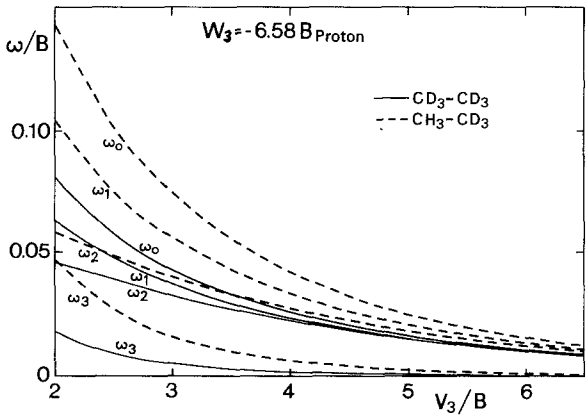

Fig. 2. Tunneling frequencies of the molecular groundstate of CD_3-CD_3 pairs (continuous lines) and CH_3-CD_3 pairs (dashed lines) as a function of V_3 with a fixed parameter $W_3=-6.58\ B_{Proton}$. The scattering centers are the *deuterated* groups

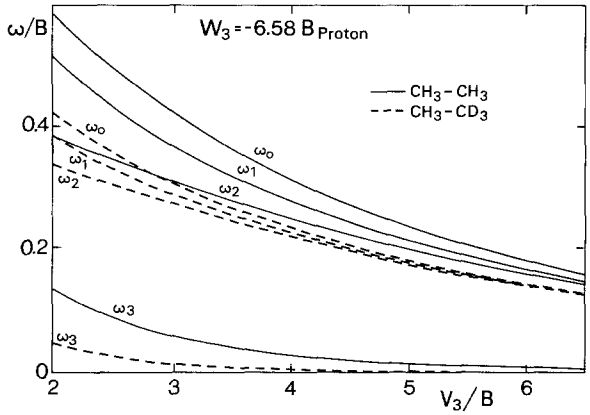

Fig. 3. Tunneling frequencies of the molecular groundstate of CH_3-CH_3 pairs (continuous lines) and CH_3-CD_3 pairs (dashed lines) as a function of V_3 with a fixed parameter $W_3=-6.58\ B_{Proton}$. The scattering centers are the *protonated* groups

IN10 and IN13 at the HFR of the ILL in Grenoble [20]. Energy resolutions from 0.15 to 12 μeV (HWHM) were used depending on the shape of the scattering laws. The IN10 (IN13) experiments were performed at an average momentum transfer of 1.7(4) $Å^{-1}$.

Spectra of LIAC with fully protonated and fully deuterated methyl groups are compared in Fig. 4. A strong isotope effect is observed: the double peak structure in the spectrum of the protonated compound shifts from 270 μeV to 12.5 μeV in the deuterated compound. As mentioned in the introduction simple scaling with the different rotational constants would predict a tunnel frequency around 25 μeV for the deuterated LIAC compound. The inelastic intensity at 12.5 μeV has a double peak structure with a splitting of about 1 μeV. The continuous lines in Figs. 4a and 4b are the result of a model calculation which will be discussed in Sect. 4. Additional measurements

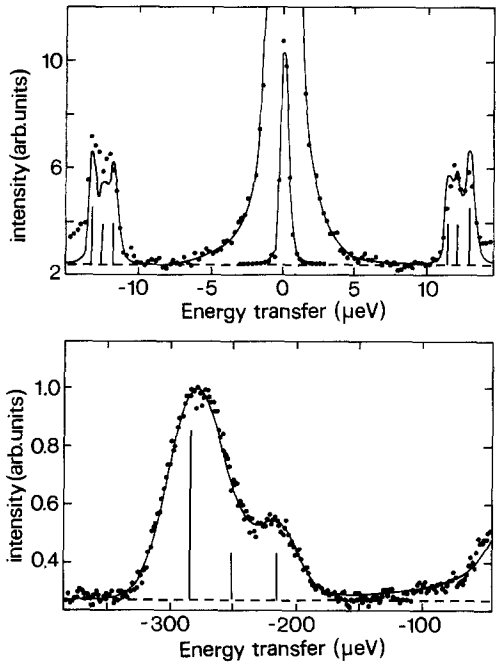

Fig. 4a and b. Tunneling spectra of (**a**) CD_3 groups in $LIAC^{(D)}$ (CD_3 $COOLi^7 \cdot 2D_2O$) measured on IN10 and (**b**) CH_3 groups in $LIAC^{(H)}$ (CH_3 $COOLi^7 \cdot 2D_2O$) measured on IN13. The calculated lines, weighted with appropriate temperature factors are inserted

with the deuterated sample with an increased energy range up to 400 μeV and with an energy resolution of 10 μeV did not reveal any other observable peaks.

Figure 5 shows IN13 spectra of mixed LIAC samples with different concentrations c of protonated methyl groups. The following trends are observed:

1. At small concentrations c a rather narrow peak occurs at 130 μeV with a weak shoulder at 180 μeV.

2. Both features shift to higher energy transfers with increasing concentration c and the shoulder grows in intensity. The dominant component broadens.

3. The shoulder becomes the dominant feature for CH_3 concentrations above 66%.

4. All spectra have intensity at smaller energy transfers ($\hbar\omega < 100$ μeV). This is mainly due to the tail of the resolution function.

All these observations on the mixed compounds can be explained qualitatively by the following picture:

In the case of small CH_3 concentrations c we have mainly CD_3-CD_3 pairs ("pure pairs", concentration $(1-c)^2$), only a few CH_3-CH_3 pairs ("pure pairs", concentration c^2) and a substantial number of CD_3-CH_3 pairs ("mixed pairs", concentration $2c(1-c)$).

We know that the tunnel frequency of the fully deuterated LIAC compounds occurs at 12.5 μeV. Therefore the spectra of the mixed compounds must be due to excitations of the pure CH_3-CH_3 pairs and mixed CD_3-CH_3 pairs.

At small concentrations c we see mainly the scattering from the mixed pairs. So we associate the dominant feature to the mixed pairs and the shoulder to

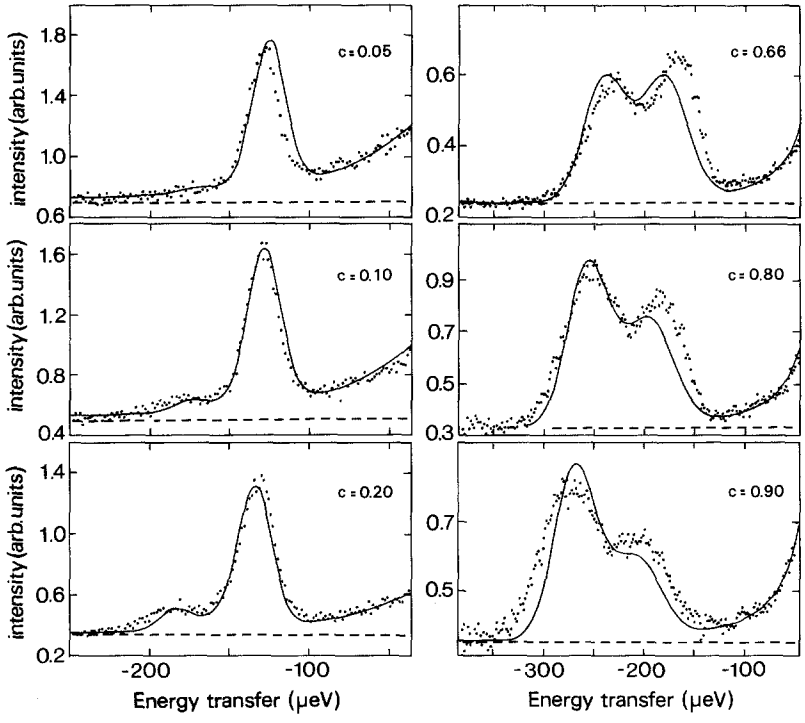

Fig. 5. Tunneling spectra from mixed LIAC samples $Li(CH_3)_c(CD_3)_{1-c} \cdot 2D_2O$ measured on IN13

the pure, protonated pairs. The fact that the excitations occur at much smaller frequencies than those in the fully protonated compound is explained by a stronger hindering potential V_3 in the deuterated compound. These very qualitative statements will be quantified by a model calculation presented in the next section.

4. Discussion

4.1. LIAC *with only* CH_3 *groups* ($LIAC^{(H)}$)

The spectrum of $LIAC^{(H)}$ (see Fig. 4) is in good agreement with results from preceeding publications [3, 5]. We will use this spectrum and the one of $LIAC^{(D)}$ as reference spectra for the mixed compounds. The continuous line in Fig. 4 is the result of a fit with three convolution broadened Gaussians. The relevant fit parameters are given in Table 3.

The parameter pair (V_3, W_3) in model (1) which gives frequencies as close as possible to the experimental values is:

$$V_3 = 3.04\, B_{\text{proton}}$$

$$W_3 = -6.2\, B_{\text{proton}}$$

These values are slightly different from those originally proposed by Clough et al. [3], which were also used in later publications [5, 7] and which produce frequencies given in Table 3 in brackets. The spin temperature T_s extracted from the intensity ratio $I_0:I_1:I_2 = 2:\varepsilon_0:\varepsilon_0$ yielded a value $T_s = 5.4\text{ K} + 0.2\text{ K}$ for our results compared to the sample temperature of 4.0 K. According to results of McDonald [21] the spin conversion time τ_s of $LIAC^{(H)}$ should be of the order of one hour at 4.2 K. As the typical measurement time for one spectrum was 24 h in our case we would have expected a fully converted sample, i.e. $T_s = T_{\text{sample}}$.

4.2. LIAC *with* CD_3 *groups only* ($LIAC^{(D)}$)

The spectrum of $LIAC^{(D)}$ has a double peak excitation at 12.5 μeV compared to an excitation around 25 μeV calculated from Hamiltonian (1) with the same pair (V_3, W_3) as used to describe the results from $LIAC^{(H)}$ but with the appropriate rotational constant. Obviously the potential barrier hindering rotation must be higher in $LIAC^{(D)}$ than in $LIAC^{(H)}$. Therefore we tried to find a parameter pair (V_3, W_3) which produces frequencies as close as possible to the observed ones. Experimentally we have essentially two observed parameters, the center of gravity of the excitation and its overall width. The second parameter is rather sensitive to W_3: A small value of W_3 gives also a small overall width. Table 4 shows calculated tunnel frequencies for given (V_3, W_3) pairs selected such that the average frequency is not far from the observed value.

Using the parameter pair ($4.47\, B_{\text{proton}}$, $-6.6\, B_{\text{proton}}$) we calculated the frequency spectrum with the following assumptions:

1. No intrinsic width of the individual peaks.
2. Intensity ratio $I_0:I_1:I_2 = 11:8:8$. No Boltzmann factors were included because $\hbar\omega_0^d/k_B T \ll 1$.

The continuous line in Fig. 4 (upper part) represents the result of this procedure. The agreement between theory and experiment is quite good. A parameter pair ($4.8\, B_{\text{proton}}$, $-6.0\, B_{\text{proton}}$) gives an inelastic structure which is too narrow. From that we conclude that a model in which the interaction potential W_3 is similar for the deuterated and protonated compound but in which the single particle potential is strongly enhanced in the deuterated compound gives a good description of the isotope effect. In order to corroborate this conclusion we tried to describe the spectra of the mixed samples on the basis of the same hypothesis.

Table 3. Measured and calculated characteristics of the tunneling spectrum of $LIAC^{(H)}$. The observed intensities correspond to a spin temperature $T_s = 5.4$ K

Peak N°	Measured Frequency (μeV)	Calculated Frequency (μeV)	Intensity	HWHM (μeV)
0	283±2	282 (279)	2.0	21±2
1	250±2	246 (242)	0.54±0.01	21±2
2	214±2	212 (204)	0.54±0.01	15±2

Table 4. Tunneling frequencies of pairs of CD_3 in μeV for various parameter pairs (V_3, W_3) in units of B_{proton}

V_3 \ W_3	−6.6	−6.2	−6.0
4.0	14.1	15.6	16.4
	15.1	16.6	17.4
	16.4	17.9	18.7
4.4	12.2	13.4	14.1
	12.8	14.0	14.7
	13.6	14.9	15.5
4.8	10.4	11.5	12.0
	10.8	11.9	12.4
	11.4	12.5	13.05

4.3. LIAC *with* CD_3 *and* CH_3 *groups*

The following model assumptions were made:

1. The samples are homogeneous mixtures.

2. No preferential pairing between the two species CD_3 and CH_3 should exist. Therefore the concentrations of the 3 different kinds of pairs are as given in Sect. 3.

3. The spectra are produced by an additive superposition of two contributions:

a) Scattering from the pure CH_3-CH_3 pairs.

b) Scattering from the mixed CH_3-CD_3 pairs.

4. Scattering contributions from the CD_3 groups are neglected because of the 46 times smaller spin dependent scattering cross section of the D nucleus compared to the proton.

5. The relative ratio between scattering from the pure and mixed pairs is calculated from the concentration c on the assumption that a pure pair scatters twice as much as a mixed one.

6. The ratio of the peak intensities for the different kinds of pairs is given by (14). The spin temperature was assumed to be 5.4 K for all spectra. That implies that all samples have the same spin conversion time and that they have been cooled down in the same manner.

7. The tunnel frequencies are calculated for pure and mixed pairs for model Hamiltonian (1) with the following hindering potential:

a) Concentration dependent single particle potential

$$V_3 = V_3^{(H)} \cdot c + V_3^{(D)}(1-c)$$

with $V_3^{(H)} = 3.04\, B_{\text{proton}}$

$V_3^{(D)} = 4.4\, B_{\text{proton}}$

b) Concentration dependent interaction potential

$$W_3 = W_3^{(H)} \cdot c + W_3^{(D)}(1-c)$$

with $W_3^{(H)} = -6.2\, B_{\text{proton}}$

$W_3^{(D)} = -6.6\, B_{\text{proton}}$

8. The line shape for the six inelastic peaks is chosen to be Gaussian, convoluted with the measured resolution function. The line widths were chosen to be 3 μeV for the low concentration spectra ($c=0.05$, 0.1 and 0.2) and 20 μeV for the others.

9. The long tail of the elastic peak is simulated by a Lorentzian centered at $\hbar\omega = 0$.

The continuous lines in Fig. 5 are the result of these model calculations. The only adjustable parameters are an energy transfer independent background, a weight of the elastic peak and an overall intensity scaling factor. Apparently the model describes quite well the trend in the concentration dependence and the positions of the peaks. The line shapes are not so well reproduced however, a fact which is not surprising in view of the very simplifying assumptions which have been made. For example, the influence of concentration fluctuations has been completely ignored. They would give rise to line broadening effects. Furthermore we used intensity ratios calculated on the basis of high barrier to rotation which is not the case in LIAC.

We would like to mention that results on $\text{LIAC}^{(H)}$ under pressure [4] are consistent with a more or less pressure independent interaction potential W_3 and a pressure dependent single particle potential which is enhanced to 4.4 B_{proton} for an externally applied pressure of about 4 kbar. This is another example of the analogy between the isotope effect and the pressure dependence of tunneling for the study of intermolecular potentials [14].

4.4. *Phonon mediated coupling of different methyl pairs*

We have seen that the single particle potential is strongly increased in $\text{LIAC}^{(D)}$ compared to $\text{LIAC}^{(H)}$. In this section we would like to show that coupling of the rotors to lattice displacements could be responsible for this effect. In order to elucidate the essential argument for phonon mediated coupling, we consider two single and equivalent methyl groups rather than two pairs of methyl groups for the sake of simplicity. Both methyl groups should be coupled to lattice vibrations. The corresponding model Hamiltonian is given by [22, 23]:

$$H = H_1 + H_2 + H_{\text{phonon}} + H_{\text{rotor phonon}} \tag{15}$$

with

$$H_{\text{phonon}} = \sum_k \left\{ \frac{p_k^2}{2m_k} + \frac{m_k}{2}\omega_k^2 x_k^2 \right\} \tag{16}$$

$$H_{\text{rotor phonon}} = \sum_k \sqrt{\frac{2m_k\omega_k}{\hbar}}\, x_k \cdot \left\{ \frac{g_k^s}{\sqrt{2}} (\sin 3\phi_1 + \sin 3\phi_2) + \frac{g_k^c}{\sqrt{2}} (\cos 3\phi_1 + \cos 3\phi_2) \right\} \tag{17}$$

H_1 and H_2 are defined by (2).

The rotor phonon coupling proportional to g_k^s is called the 'shaking' term, the one proportional to g_k^c the 'breathing' term. The denominator $\sqrt{2}$ occurs because two methyl groups are involved here.

Treating Hamiltonian (15) in Hartree approximation for the librational groundstate we find for the mean displacement of the k^{th} normal mode:

$$\langle x_k \rangle = -\mathscr{C} \frac{g_k^c}{\hbar \omega_k} \sqrt{\frac{\hbar}{m_k \omega_k}},$$

$$\mathscr{C} = \sum_{i=1}^{2} \langle 0_i \Gamma_i | \cos 3\phi_i | 0_i \Gamma_i \rangle \leqq 0 \tag{18}$$

$|n_i \Gamma_i\rangle$ are eigenstates of the effective Hamiltonian H_i^{eff} in Hartree approximation ($n=0$ means the librational ground state):

$$H_i^{\text{eff}} = -B_i \frac{\partial^2}{\partial \phi_i^2} + V_3 \cos 3\phi_i - \mathscr{C} \sum_k \frac{(g_k^c)^2}{\hbar \omega_k} \cos 3\phi_i - \mathscr{C} \sum_k \frac{g_k^c g_k^s}{\hbar \omega_k} \sin 3\phi_i + \tfrac{1}{4} (\mathscr{C})^2 \sum_k \frac{(g_k^c)^2}{\hbar \omega_k} \tag{19}$$

The matrix elements $\langle 0\Gamma | \cos 3\phi | 0\Gamma \rangle$ are plotted in Fig. 6 as a function of V_3/B. The corresponding matrix elements $\langle 0\Gamma | \sin 3\phi | 0\Gamma \rangle$ are zero.

For small V_3/B values we have a pronounced variation of $\langle 0\Gamma | \cos 3\phi | 0\Gamma \rangle$ with V_3/B and with Γ. In that case deuteration of the second rotator increases

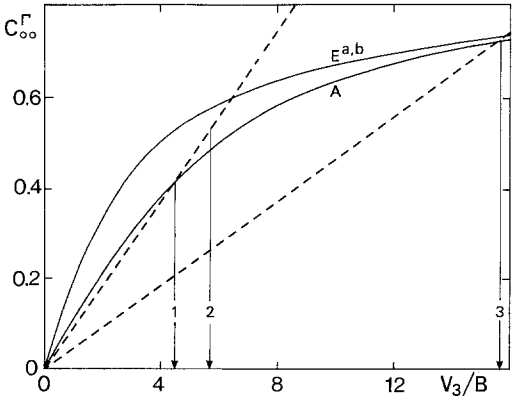

Fig. 6. Expectation value $\langle 0\Gamma | \cos 3\phi | 0\Gamma \rangle$ of the operator $\cos 3\phi$ in the librational ground state ($C_{00} := -\langle 0\Gamma | \cos 3\phi | 0\Gamma \rangle$). The second arrow indicates the $V_3^{\text{eff}}/B_{\text{proton}}$ value that corresponds to a tunneling frequency of 270 μeV, the third arrow indicates the self-consistently obtained $V_3^{\text{eff}}/B_{\text{deuteron}}$ value when the surrounding is completely deuterated as described in the text. The first arrow shows the low temperature value for $V_3^{\text{eff}}/B_{\text{proton}}$

the effective single particle potential of the first rotator (cf. (18, 19)). A similar effect is produced if an A type neighbour is replaced by an E^a or E^b type neighbour. At higher barriers ($V_3/B > 15$) these effects become negligible.

In the real system of course we have to consider a large number of rotators which are statistically distributed with respect to their isotope and symmetry type. As long as the translational symmetry is not broken too seriously we expect that the effective single particle potential depends only on the averaged concentration of the surrounding species. For large numbers N of rotators we may neglect the selfconsistent adjustment of

$$\mathscr{C} = \sum_{i=1}^{N} \langle 0_i \Gamma_i | \cos 3\phi_i | 0_i \Gamma_i \rangle$$

(then the last summand in (19) becomes an unimportant additive constant) due to a symmetry change of a certain rotator (at which the neutron is scattered). Then $\mathscr{C}$ only depends on the concentration of A symmetric species and on the concentration of deuterated methyl groups.

In consequence we expect *i*) a decreasing tunneling frequency with increasing CD_3 concentration, *ii*) a more pronounced isotope shift than the usual one and *iii*) a tunneling frequency that depends on the averaged symmetry type of the surrounding. All 3 effects are observed in LIAC ([5], and present paper).

If we try to represent each rotator pair in LIAC by one methyl group in an orientational potential $V_3^{\text{eff}} = 5.67\, B_{\text{proton}}$ (corresponding to 270 μeV tunneling splitting) then the thermal averaged $\overline{\langle 0\Gamma | \cos 3\phi | 0\Gamma \rangle} = \mathscr{C}/N$ would be 0.525 (Fig. 6). If we furthermore assume for the 3-fold potential V_3 in (15) to be zero (which would mean, that the effective single particle potential should be attributed solely to the described displacement of breathing-type phonon modes, i.e. the rotators are "digging" their own 3-fold orientational potential hole within their distortable surrounding – this assertion corresponds to the observed 6 fold crystallographic symmetry along the methyl axis in LIAC [8]), then

$$V_3^{\text{eff}} = -2\,\overline{\langle 0\Gamma | \cos 3\phi | 0\Gamma \rangle} \cdot \left[\left(\sum_k \frac{(g_k^c)^2}{\hbar \omega_k} \right)^2 + \left(\sum_k \frac{g_k^c g_k^s}{\hbar \omega_k} \right)^2 \right]^{1/2} \tag{20}$$

i.e. $V_3^{\text{eff}} \propto \overline{\langle 0\Gamma | \cos 3\phi | 0\Gamma \rangle}$ where for equal population of the librational ground states the slope is determined by the average value of the matrix elements $\langle 0A | \cos 3\phi | 0A \rangle$ and $\langle 0E | \cos 3\phi | 0E \rangle$ (dashed line in Fig. 6). Now deuteration implies a scaling of all

energy quantities by a factor 2, therefore we get half a slope for the $V_3^{\text{eff}} \propto \langle 0\Gamma|\cos 3\phi|0\Gamma\rangle$ proportionality in Fig. 6 (possible modifications of the phonon spectrum ignored!). The selfconsistent value of V_3^{eff} (deuterated surrounding) is now 7.85 B_{proton}, corresponding to a tunneling frequency of 170 μeV i.e., the shift is comparable to the observed one. As the slope of $\langle 0\Gamma|\cos 3\phi|0\Gamma\rangle$ does not vary much between $V_3 = 5.67\ B_{\text{proton}}$ and $V_3 = 7.85\ B_{\text{proton}}$ we can justify the linear interplation of V_3 with concentration of deuterated methyl groups in Sect. 4.3. On the other hand: A reduction of the spin temperature (only A-symmetric methyl groups in the crystal) means that $\langle 0\Gamma|\cos 3\phi|0\Gamma\rangle = \langle 0A|\cos 3\phi|0A\rangle$ and the selfconsistence requirement yields a new V_3^{eff} of almost 4.53 B_{proton}, corresponding to 344 μeV tunneling frequency. Also this shift in tunneling frequency has the correct order of magnitude [5].

This coarse estimation merely should make clear, how variing degrees of lattice distortions due to varing orientational localisation of the rotators could react back upon the rotators. Not too high orientational potentials (in case of methyl groups corresponding to tunneling frequencies larger than 50 μeV) and sufficiently strong breathing type-coupling to the phonon bath may result in an uncommon isotopic shift and in an increasing tunneling frequency at (spin-) temperatures below the tunneling frequency.

5. Conclusions

The isotope effect of tunneling motions of coupled groups of methyl groups has been studied theoretically and experimentally by high resolution inelastic neutron scattering. The observed isotope effect is by a factor two stronger than expected on the basis of a simple scaling of the hindering potential by the rotational constants. This excess isotope effect can be explained by the assumption of a strongly increased single particle potential in LIAC$^{(D)}$ compared to LIAC$^{(H)}$ and an interaction potential which is nearly independent of the isotopic species. On the basis of this hypothesis it is also possible to explain qualitatively the concentration dependence of spectra of the LIAC samples consisting of isotopic mixtures. The strong increase of the single particle potential by deuteration was tentatively explained by phonon mediated coupling, which predicts that such unusual isotope effects should only occur in systems with CH_3 tunneling frequencies well above 50 μeV and sufficiently strong breathing type coupling to the phonons.

The authors are grateful to R. Scherm and A. Hüller for many stimulating discussions. They thank J.F. Barthelemy and P. Joubert-Bousson for their help in preparing the experiments.

References

1. Allen, P.S., Branson, P.: J. Phys. C **11**, L121 (1978)
2. Allen, P.S.: Faraday Symp. Chem. Soc. **13**, 133 (1978)
3. Clough, S., Heidemann, A., Horsewill, A.H., Paley, M.N.J.: Z. Phys. B – Condensed Matter **55**, 1 (1984)
4. Heidemann, A., Eckert, J., Passell, L., Häusler, W.: Z. Phys. B – Condensed Matter **66**, 75 (1987)
5. Heidemann, A., Abed, K.J., Barker, C.J., Clough, S.: Z. Phys. B – Condensed Matter **66**, 355 (1987)
6. Crits, E., Van Gerven, L., Emid, S.: Physica B**150**, 329 (1988)
7. Häusler, W., Hüller, A.: Z. Phys. B – Condensed Matter **59**, 177 (1985)
8. Galigné, J.L., Mouvet, M., Falgueirettes, J.: Acta Crystallogr. B**26**, 368 (1970)
9. Alefeld, B., Anderson, I.S., Heidemann, A., Magerl, A., Trevino, S.F.: J. Chem. Phys. **76**, 2758 (1981)
10. Cavagnat, D., Magerl, A., Vettier, C., Anderson, I.S., Trevino, S.F.: Phys. Rev. Lett. **54**, 193 (1985)
11. Cavagnat, D., Magerl, A., Vettier, C., Clough, S.: J. Phys. C**19**, 6665 (1986)
12. Heidemann, A., Prager, M., Monkenbusch, M.: Z. Phys. B – Condensed Matter **76**, 77 (1989)
13. Heidemann, A., Lushington, K.J., Morrison, J.A., Neumaier, K., Press, W.: J. Chem. Phys. **81**, 5799 (1984)
14. Prager, M., Press, W., Heidemann, A.: J. Chem. Phys. **75**, 1442 (1981)
15. Wilson, E.B., Jr.: J. Chem. Phys. **2**, 276 (1935)
16. Clough, S., Heidemann, A., Paley, M.: J. Phys. C**13**, 4009 (1980)
17. Press, W.: Single-particle rotations in molecular crystals. In: Springer Tracts in Modern Physics. Vol. 92. Berlin, Heidelberg, New York: Springer 1981
18. Prager, M., Heidemann, A., Häusler, W.: Z. Phys. B – Condensed Matter **64**, 447 (1986)
19. Heidemann, A.: Quantum aspects of molecular motions in solids. In: Springer Proceedings in Physics. Heidemann, A., Magerl, A., Prager, M., Richter, D., Springer, T. (eds.), Vol. 17, p. 44. Berlin, Heidelberg, New York: Springer 1987
20. Maier, B.: Neutron beam facilities at the HFR Grenoble (1988). Copies may be obtained from the Scientific Secretary, ILL, 156X, F 38042 Grenoble, Cedex, France
21. Mc Donald, P.: Thesis, Nottingham (1984)
22. Prager, M., Stanislawski, J., Häusler, W.: J. Chem. Phys. **86**, 2563 (1987)
23. Hewson, A.C.: J. Phys. C**15**, 3841, 3855 (1982)
24. Heidemann, A., Anderson, I., Jeffryes, B., Alefeld, B.: Z. Phys. B – Condensed Matter **49**, 123 (1982)

A. Heidemann
Institut Max von Laue – Paul Langevin
Avenue des Martyrs – 156X
F-38042 Grenoble Cedex
France

H. Friedrich
E. Günther
Physikalisch-Technische Bundesanstalt Braunschweig
Bundesallee 100
D-3300 Braunschweig
Federal Republic of Germany

W. Häusler
Institut für Theoretische Physik I
Universität Erlangen-Nürnberg
Glückstrasse 6
D-8520 Erlangen
Federal Republic of Germany